

Signatures of Quantum Coherences in Rydberg Excitons

P. Grünwald,^{1,*} M. Abmann,² J. Heckötter,² D. Fröhlich,² M. Bayer,² H. Stolz,¹ and S. Scheel¹

¹*Institut für Physik, Universität Rostock, Albert-Einstein-Strasse 23, D-18059 Rostock, Germany*

²*Experimentelle Physik 2, Technische Universität Dortmund, D-44221 Dortmund, Germany*

Coherent optical control of individual particles has been demonstrated both for atoms and semiconductor quantum dots. Here we demonstrate the emergence of quantum coherent effects in semiconductor Rydberg excitons in bulk Cu₂O. Due to the spectral proximity between two adjacent Rydberg exciton states, a single-frequency laser may pump both resonances with little dissipation from the detuning. As a consequence, additional resonances appear in the absorption spectrum that correspond to dressed states consisting of two Rydberg exciton levels coupled to the excitonic vacuum, forming a V-type three-level system, but driven only by one laser light source. We show that the level of pure dephasing in this system is extremely low. These observations are a crucial step towards coherently controlled quantum technologies in a bulk semiconductor.

Introduction. Rydberg atoms are understood to be those whose valence electron has been promoted to a quantum state with principal quantum number $n \gg 1$. These exotic quantum states feature large coupling strengths to other Rydberg states and extremely long life times (scaling with n^2 and $n^{3\cdots 4.5}$, respectively), making them an excellent choice for the study of quantum aspects of light-matter interaction [1]. Rydberg atoms have been used in the first direct observation of quantum collapses [2] as well as quantum non-demolition experiments [3]. In recent years, they have matured into a promising platform for quantum information research [4].

Rydberg physics is not confined to the realm of atomic physics. Recently, Rydberg states with principal quantum numbers up to $n = 25$ were observed in the semiconductor Cu₂O [5]. Here, Mott-Wannier excitons, bound states of electrons and holes, substitute for real atoms. A number of concepts developed within the framework of Rydberg atoms are displayed by these exotic states, such as typical scaling laws for the natural linewidth or the oscillator strength ($\propto n^{-3}$ [6, 7]). Additionally, a quantum defect associated with an effective quantum number $n^* = n - \delta_\ell$ [8] was observed and shown to be mainly due to the nonparabolicity of the valence bands [9, 10].

A hitherto unexplained feature is the appearance of additional resonances in the absorption spectra of Rydberg excitons for principal quantum numbers larger than $n \gtrsim 12$ (see Fig. 1). They occur halfway between each pair of excitonic resonances after excitation with a narrow-bandwidth laser, but vanish for large laser powers, where Rydberg blockade sets in. These resonances constitute a significant deviation from simple Rydberg models, as well as established methods of many-body physics [9–13]. We will demonstrate here that they represent coherent (quantum) interactions between exciton states of different principal quantum numbers.

In the following, we consider quantum coherence in terms of the off-diagonal elements of the density matrix in Fock basis. An effect is based on quantum coherence if these off-diagonal elements are a necessary constituent of said effect. For open quantum systems, and in particular for the emission of light from a given source, this is achieved using a dominant coherent drive of the source of the emission. Such a dominance is usually diminished by dissipative effects such

as energy and phase relaxation (dephasing). Semiconductor systems are typically prone to strong phase relaxations due to phonon coupling and other many-body effects. Nevertheless, in low-dimensional systems such as quantum dots in microcavities, quantum coherent processes have been observed [14–16]. However, so far no such coherent effects could be demonstrated in bulk systems such as those used for Rydberg-exciton generation.

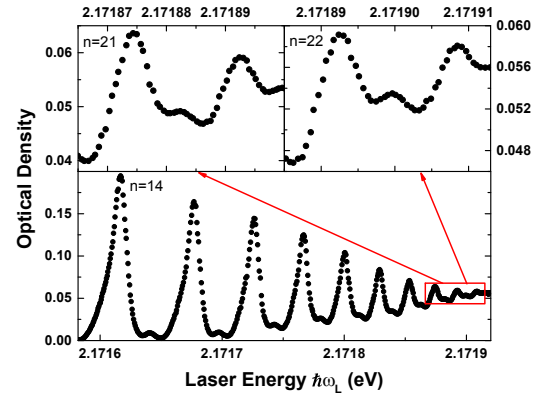


FIG. 1. Experimental absorption spectra showing additional resonances between isolated Rydberg exciton resonances.

The quantitative description of absorption and emission processes in semiconductors generally requires both the medium properties as well as a quantum-optical description of the emitters, here the excitons. For example, the fluorescent emission of a coherently pumped quantum well required the combination of both the absorption (not to be confused with the absorption spectrum) as well as the spectral intensity distribution of the excitons [17, 18]. In that case, the necessity to combine both processes follows from Kirchhoff's law [19] and from the quantum-optical input-output relations [20]. More recently, such an approach has also been applied to highly doped quantum wells in thermal pumping [21]. Using a similar approach, it becomes possible to infer that quantum coherence has been achieved in Rydberg exciton systems directly from the experimental absorption spectra.

Absorption Spectra. The absorption spectrum of a semiconductor is commonly measured via a frequency-insensitive detector such as a photodiode placed behind the sample. This device registers the spectrally integrated transmission of light, which is then compared to the full laser intensity impinging on the crystal. A spectral distribution as shown in Fig. 1 is obtained as a function of the laser frequency ω_L . The lost intensity is often assumed to be equal to the absorption, thereby neglecting secondary emission and losses due to scattering. The commonly applied model for the absorption spectrum $a(\omega)$ of an exciton with principal quantum number n follows the Toyozawa formula [22]

$$a(\omega) = C_n \frac{\frac{\Gamma_n}{2} - 2q_n(\omega_n - \omega)}{\left(\frac{\Gamma_n}{2}\right)^2 + (\omega_n - \omega)^2}, \quad (1)$$

where C_n is proportional to the oscillator strength and ω_n and q_n are the resonance frequency of the exciton and the asymmetry parameter of the line shape, respectively. The natural linewidth Γ_n should scale with n^{-3} , as known from atomic systems. According to Elliott [6], in Cu_2O one also observes $C_n \propto n^{-3}$.

However, Eq. (1) only describes the probability density of absorbing a photon at frequency ω by the crystal, whereas the measurement setup detects the transmitted light as well as contributions from resonance fluorescence, which includes light scattered or reemitted along the forward direction. Therefore, in the event that a photon is indeed absorbed, $a(\omega)$ is scaled by the resonance fluorescence contributions from the excitons $I_X(\omega, \omega_L)$ [23]. That scaled spectrum impinges on the frequency-insensitive detector yielding a spectrum

$$A(\omega_L) = \int_{-\infty}^{\infty} d\omega a(\omega) I_X(\omega, \omega_L). \quad (2)$$

The determined ‘‘absorption’’ spectrum of the Cu_2O crystal thus also contains components from coherent and incoherent emissions of the sample. Here the coherent contributions correspond to phase-preserving elastic scattering processes, which replicate the excitation field. Meanwhile, the incoherent contributions include inelastically scattered fields, which can result, for example, in the appearance of the Moll-triplet for large Rabi frequencies [24].

$I_X(\omega, \omega_L)$ is determined by the spectral intensity distribution of the excitons $S_X(\omega, \omega_L)$ via

$$I_X(\omega, \omega_L) = g^2 S_X(\omega, \omega_L), \quad (3)$$

with g being proportional to the dipole transition moment d between the excitonic and vacuum states. In turn, $S_X(\omega, \omega_L)$ is directly connected to the quantum optical dynamics of the exciton states driven by the laser beam. Modelling adequately the quantum states involved in excitation and relaxation processes hence suffices to determine $A(\omega_L)$ and compare with the experiments.

Master Equation Approach. In order to obtain the correct exciton dynamics, we employ the following description. A single exciton resonance is modeled by only two states, the excited state $|n\rangle$ and the excitonic vacuum $|0\rangle$ as the ground state. Both states are dipole-coupled (dipole moment d_n) by the pump laser with Rabi frequency Ω_n . Further, the excited state undergoes radiative, Markovian damping with energy relaxation rate Γ_n . According to standard Wigner–Weißkopf theory for the damping, we find that

$$\Gamma_n \propto d_n^2 \propto n^{-3}, \quad \Omega_n \propto d_n \propto n^{-3/2}. \quad (4)$$

The Hamiltonian and the corresponding master equation for the density operator follow a Bloch theory:

$$\begin{aligned} \hat{H}_n &= \hbar \left[\delta_n \hat{A}_{n,n} + \Omega_n (\hat{A}_{0,n} + \hat{A}_{n,0}) \right], \\ \frac{d\hat{\rho}_n}{dt} &= \frac{1}{i\hbar} [\hat{H}_n, \hat{\rho}_n] + \frac{\Gamma_n}{2} \mathcal{L}_{\hat{A}_{0,n}}[\hat{\rho}_n], \\ \mathcal{L}_{\hat{X}}[\hat{\rho}] &= 2\hat{X}\hat{\rho}\hat{X}^\dagger - \hat{X}^\dagger\hat{X}\hat{\rho} - \hat{\rho}\hat{X}^\dagger\hat{X}, \end{aligned} \quad (5)$$

with $\hat{A}_{j,k} = |j\rangle\langle k|$ being the excitonic operators and $\delta_n = \omega_n - \omega_L$. Here, $\mathcal{L}_{\hat{X}}$ describes the Lindblad term for operator \hat{X} , in this case the exciton annihilation operator $\hat{A}_{0,n}$.

It is instructive to discuss the limit of weak light-matter coupling first, as that is usually expected in these experiments. For low excitation, $\langle \hat{A}_{n,n} \rangle \ll 1$, the incoherent spectral components from the excitons can be neglected as well as excitation-induced dephasing via exciton-exciton scattering. Thus, the spectral distribution of the excitons reduces to a Rayleigh component [25] $S_X(\omega, \omega_L) = |\mathcal{C}|^2 \delta(\omega - \omega_L)$, where $|\mathcal{C}|^2$ is the coherent part of the exciton intensity. Thus, we find in this limit

$$A(\omega_L) = g^2 |\mathcal{C}|^2 a(\omega_L), \quad (6)$$

meaning that fitting the observed spectra in Ref. [5] to Eq. (1) is sufficiently accurate if $g^2 |\mathcal{C}|^2$ can be regarded as insensitive to variations of the laser frequency and the principal quantum number n . For higher laser powers with respect to the light-matter couplings, this condition becomes invalid and $|\mathcal{C}|^2$ must be investigated in more detail. In the steady-state solution of Eq. (5), $|\mathcal{C}|^2 = |\langle \hat{A}_{n,0} \rangle|^2 \approx \langle \hat{A}_{n,n} \rangle$, and the measured absorption spectrum becomes

$$A(\omega_L) = g^2 \Omega_n^2 C_n \frac{\frac{\Gamma_n}{2} - 2q_n \delta_n}{\left[\left(\frac{\Gamma_n}{2}\right)^2 + 2\Omega_n^2 + \delta_n^2\right]^2}. \quad (7)$$

Comparing Eq. (7) with Eq. (1), a few results should be noted. First, the oscillator strength is calculated by integrating an absorption peak over all laser frequencies ω_L . In the linear regime, where $\Omega_n \ll \Gamma_n$, all n -dependencies apart from C_n cancel out in the integrated transmission. Thus, the expected n^{-3} -dependence of the oscillator strength is precisely what is observed in the experiment. Second, the corrected line shape of the spectrum differs slightly from the Toyozawa formula, with the denominator being squared. This yields deviations to

the fit parameters q_n and Γ_n in a least-squares fit. The line shape of isolated resonances can be fitted well to both models, Eqs. (1) and (7), making a differentiation impossible (see SOM). This means that our corrected model can fully explain the standard Toyozawa line shape observed in earlier experiments. Overall we can conclude that, in the linear regime and considering only isolated resonances, we find no indication of additional resonances.

Third, and notwithstanding the previous statements the approximation of using solely Toyozawa's formula breaks down, however, when reaching the nonlinear regime by increasing either the laser intensity or the principal quantum number n of the exciton resonance. For $\Omega_n \lesssim \Gamma_n$, power broadening sets in, yielding a perceived larger line width and a steeper slope for the fitted oscillator strength. Given the scaling $\Omega_n/\Gamma_n \propto n^{3/2}$ from Eq. (4), in the strong-coupling limit ($\Omega_n \gg \Gamma_n$) the area under the absorption peak scales as $n^{-15/2}$ compared to the n^{-3} -scaling in the weak-coupling regime.

Additional resonances in the absorption spectrum. At intermediate excitation strengths $\Omega_n \lesssim \Gamma_n$, the incoherent part of the exciton spectrum becomes relevant, i.e. $S_X(\omega, \omega_L)$ is no longer proportional to a δ -distribution but instead broadens. The incoherent spectrum of a single two-level system and its quantum features are well documented in the literature [26, 27]. One may assume that the additional resonances result from strong-coupling effects, representing light-matter dressed states. However, at the given laser intensities, we are not yet in the strong-coupling regime, and thus, only a single peak occurs in the exciton spectrum for one isolated Rydberg resonance. Additional peaks resulting from strong coupling effects would show different spectral behaviour, such as the Mollow-triplet. Hence, an isolated exciton state n is insufficient to explain the additional resonances.

However, excitons with large n can no longer be considered spectrally isolated, see Fig. 1. These resonances are spectrally close, e.g., $|\omega_{15} - \omega_{16}| \approx 49 \mu\text{eV}/\hbar = 12 \text{ GHz}$. Hence, tuning the laser frequency around a high- n resonance, different states $n, n+1$ of the exciton can be populated with limited influence by the detuning. It is therefore appropriate to consider a system of two exciton states $|n\rangle$ and $|n+1\rangle$ as the possible excited states, and the excitonic vacuum $|0\rangle$ as their common ground state. The resonances do not couple directly to one another but they are dipole-coupled to the vacuum state and driven by the same laser light, yielding a V-type three-level system with a single pump laser of frequency ω_L (see Fig. 2). Note that we do not consider two excitons, but the presence of a single exciton in a system with different possible excited quantum states.

Comparing with Eq. (5), we now take into account the sum of the two Hamiltonians, \hat{H}_n and \hat{H}_{n+1} , with the correspond-

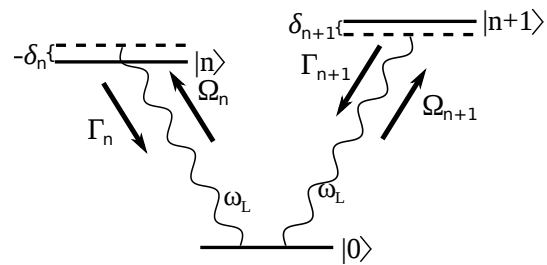


FIG. 2. Model for two Rydberg excitons with principal quantum numbers n and $n+1$, coupled to the excitonic vacuum state $|0\rangle$.

ing Lindblad terms and relaxation rates Γ_n and Γ_{n+1} :

$$\begin{aligned} \hat{H}_{3\text{LS}} &= \hat{H}_n + \hat{H}_{n+1}, \\ \frac{d\hat{\rho}_{3\text{LS}}}{dt} &= \frac{1}{i\hbar} [\hat{H}_{3\text{LS}}, \hat{\rho}_{3\text{LS}}] \\ &\quad + \frac{\Gamma_n}{2} \mathcal{L}_{\hat{A}_{0,n}}[\hat{\rho}_{3\text{LS}}] + \frac{\Gamma_{n+1}}{2} \mathcal{L}_{\hat{A}_{0,n+1}}[\hat{\rho}_{3\text{LS}}]. \end{aligned} \quad (8)$$

The common ground state $|0\rangle$ permits a transfer of an excitation from one exciton state to the other, forming an effective quadrupolar coupling, i.e. $\langle \hat{A}_{n,n+1} \rangle \neq 0$, see SOM for details. Hence, the coherent drive induces an effective transition between the exciton states, whose transition rate is directly linked to the Rabi frequencies Ω_n and Ω_{n+1} .

The incoherent part of the three-level exciton intensity spectrum $S_X(\omega, \omega_L)$ is displayed in Fig. 3 for the laser frequency $\omega_L = \frac{\omega_{15} + \omega_{16}}{2}$. With increasing Rabi frequency (curves from bottom to top), an internal resonance builds up. This resonance corresponds to a dressed state of the two excitons, formed by the effective quadrupole coupling. The measured absorption spectrum $A(\omega_L)$, following Eq. (2), now includes $S_X(\omega, \omega_L)$ from the three-level Hamiltonian and the Toyozawa formula (1). It features prominently the additional resonances from the experiments (see bottom panel in Fig. 4).

To account for the discrepancies between system parameters determined via fitting Toyozawa's formula and the complex three-level model, we apply the following rules: the decay rates Γ_n follow the basic n^{-3} law, fitted to the lower n -resonances. Deviations from this behaviour are thus thought to be included in the full description. The q_n are taken from the fit parameters. For a simple model discussion on their behaviour see the SOM. The Rabi frequencies were not fitted in [5], so we will use values that reproduce the experiments.

Further increase of the laser intensity results in two effects (see top panel in Fig. 4). First, the additional resonances develop an asymmetry towards the lower-frequency side of the spectrum. Second, for even higher field intensities, they start to disappear, while the absorption in general decreases. The former effect follows directly from our model Hamiltonian, where the combination of symmetric exciton intensity spectrum and the asymmetric Toyozawa formula tilts the additional resonances (see lower panel in Fig. 4). The regime of strong pumping is signified by the latter effect. The dressed

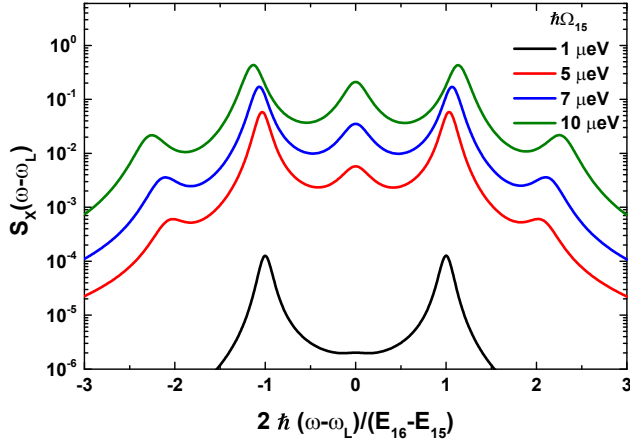


FIG. 3. Incoherent exciton-intensity spectrum $S_X(\omega)$ for two resonances with $n = 15, 16$, coupled to the excitonic vacuum with the parameters taken from Ref. [5]. The laser is tuned to the center between the resonances and the Rabi frequencies are $\Omega_{16} = \Omega_{15}(\frac{15}{16})^{3/2}$.

states are shifted out of the spectral region by the large Rabi frequency. Furthermore, for strong driving, the dipole- and quadrupole moments decrease because of the saturated level occupation. In that case, the effective system reverts back to the isolated resonance scenario. Also, at this point the Rydberg blockade sets in [5]. If one exciton is excited to a Rydberg state, the excitation of another one becomes suppressed. Note that Rydberg blockade depends strongly on parameters like sample thickness and the exact geometry used for excitation and has thus not been included in the theoretical results shown in the lower panel of Fig. 4.

So far, we have limited our discussion to energy relaxation, neglecting the influence of pure dephasing. If the additional resonances are indeed based on quantum coherent coupling of the different resonances, increasing the pure dephasing rate (by inclusion of another Lindblad term $\mathcal{L}_{\hat{A}_{n,n}}[\hat{\rho}]$ into the master equation) should influence their magnitude. Indeed, as shown in Fig. 5, already for dephasing rates close to the pumping rate, the resonances disappear. Two conclusions can be drawn from this. First, radiationless dephasing is surprisingly small in Rydberg excitons in Cu_2O and second, the additional resonances appearing between the exciton resonances are clear signatures of quantum coherence between adjacent exciton states. Remarkably, these coherences between exciton states with consecutive quantum numbers are driven by the incoherent part of the exciton spectrum instead of the coherent part, which drives the coherences between the ground state and the exciton states.

We also note that the curves for higher dephasing rates are very similar to the experimental curves for higher pumping, see top panel in Fig. 4. It seems reasonable that, when increasing the laser intensity beyond saturation, phonons become dominantly excited and induce stronger dephasing rates. This can only be better understood by a thorough analysis of

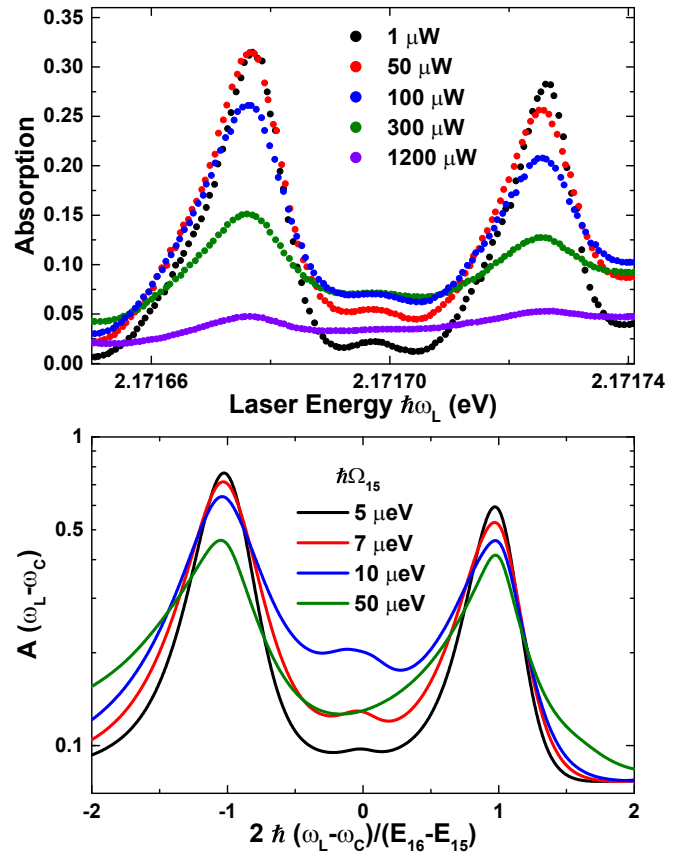


FIG. 4. Top: experimental absorption spectra for $n = 15, 16$ and different laser intensities as shown in the legend. Bottom: absorption spectrum for the two resonances $n = 15, 16$ for different Rabi frequencies with $\Omega_{16} = \Omega_{15}(\frac{15}{16})^{3/2}$.

the decay rates and Rabi frequencies present in the experiments.

Summary and Conclusions. We have analyzed the quantum coherent properties of the Rydberg exciton spectrum in Cu_2O . The observed absorption in different experimental situations includes, besides the absorption-induced attenuation, also the intensity spectrum of the Rydberg excitons. In the linear regime of a coherently driven system, this additional effect simply scales the absorption spectrum. For stronger excitation, the incoherent part of the exciton spectrum induces additional resonances, which were also observed in the experiments. Their appearance indicates the onset of measurable quantum coherence between exciton states of consecutive principal quantum number, as well as very low levels of pure dephasing.

Our model for the absorption spectrum of Rydberg excitons accounts for a number of hitherto unexplained features, which should also be applicable to a variety of similar semiconductor experiments. Rydberg excitons in Cu_2O have now reached a stage at which coherent quantum effects become visible, and the precise nature of the excitonic Hamiltonian becomes detectable. This allows for controlled quantum manipulation and

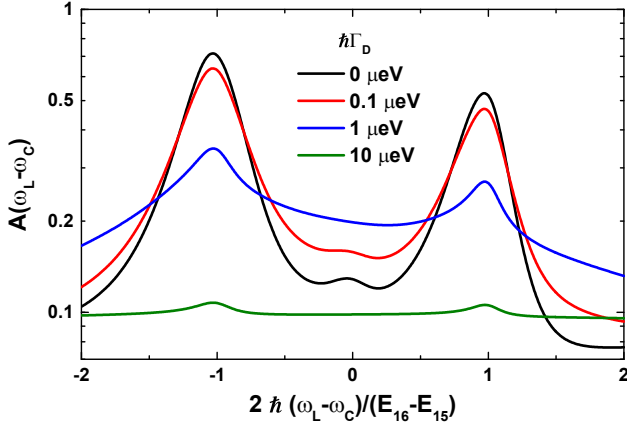


FIG. 5. Absorption spectrum for the two resonances $n = 15, 16$ for different dephasing rates Γ_D and $\hbar\Omega_{15} = 7 \mu\text{eV}$ and $\Omega_{16} = \Omega_{15}(\frac{15}{16})^{3/2}$.

state generation for excitons and opens up the possibility for developing semiconductor quantum technologies.

Acknowledgements. We gratefully acknowledge support by the Collaborative Research Centre SFB 652/3 'Strong correlations in the radiation field' and the International Collaborative Research Centre TRR 160 'Coherent manipulation of interacting spin excitations in tailored semiconductors', both funded by the Deutsche Forschungsgemeinschaft.

SUPPLEMENTAL MATERIAL

Comparison of fitted Absorption Spectra

The experimental spectra from [5] were fitted to the Toyozawa formula instead of the absorption spectrum for low driving strength, from here on denoted as Rabi spectrum, cf. Eq. (1) and (7) from the main text, respectively. Both functions may be easily fitted to the experiments. To compare them theoretically, we will use the following parameters: the apparent resonance as the maximum of the distribution, the FWHM value, and the peak area.

The maximum of the distribution is given for a certain detuning between laser and actual exciton resonance $\delta_n = \omega_n - \omega_L \neq 0$ due to the asymmetry. Hence, for $q_n \rightarrow 0$, δ_n should become 0 as well for either model function. With this in mind, we can determine the maximum unambiguously to be

$$\delta_{n,\max} = \frac{\Gamma_n}{4q_n} \left[1 - \sqrt{1 + 4q_n^2} \right] \quad (9)$$

for the Toyozawa formula and

$$\delta_{n,\max} = \frac{\Gamma_n}{6q_n} \left[1 - \sqrt{1 + 3q_n^2 \left(1 + \frac{8\Omega_n^2}{\Gamma_n^2} \right)} \right] \quad (10)$$

for the Rabi spectrum. In case of $\Omega_n \ll \Gamma_n$, we find a different relation between Γ_n and q_n , but without a theory for q_n

this can easily be included in the fit parameters. Moreover, in the region where $8\Omega_n^2/\Gamma_n^2 \approx 1$ and for $q_n \ll 1$, the maxima for both models become

$$\delta_{n,\max} \approx \frac{\Gamma_n q_n}{2}. \quad (11)$$

The FWHM value follows, after some lengthy algebra as

$$\text{FWHM}_n = \sqrt{3 + \frac{1 - \sqrt{1 + 4q_n^2}}{q_n^2} \Gamma_n} \quad (12)$$

for the Toyozawa formula. The Rabi spectrum FWHM value requires the solution of a fourth-order polynomial. More interestingly, when neglecting the asymmetry, we find for the Rabi spectral width

$$\text{FWHM}_n = \sqrt{\sqrt{2} - 1} \sqrt{\Gamma_n^2 + 8\Omega_n^2}. \quad (13)$$

Power broadening arises for sufficiently large n , whereas the overall width is scaled down by a factor of around 1.55. Crucially, the n -dependence of the linewidth for $\Gamma_n \gg \Omega_n$ is not changed as the scaling is constant. For a similar small change of the width for $q_n \neq 0$ for both model functions, we again cannot detect differences between the models for sufficiently low ratios of Ω_n/Γ_n .

Finally, the integrated peak area F_n reads as

$$F_n = \pi C_n \quad (14)$$

for the Toyozawa formula and

$$F_n = \frac{\pi}{4} \frac{\Gamma_n g_n^2 \Omega_n^2}{\left(\left(\frac{\Gamma_n}{2} \right)^2 + 2\Omega_n^2 \right)^{3/2}} C_n \quad (15)$$

for the Rabi model. Inserting the known dependencies of the different parameters we find that both scale only with C_n for low pumping strengths, while for larger ones, the Rabi area would scale with $F_n \propto n^{-9/2} C_n$. Overall, we thus deduce that for low pumping strengths no detectable difference between these models can be found by freely fitting the model parameters to the experiments. Exemplarily, we have fitted the resonance $n = 10$ in Fig. 6 with both models.

Dynamics of Three-Level-System

Applying the master equation [25] for the three-level system, Eq. (8) from the main text, we can derive the equations of motion for the relevant occupations $\langle A_{jj} \rangle$ and coherences $\langle \hat{A}_{0j} \rangle$, $j = n, n+1$, respectively, which read as

$$\frac{d}{dt} \langle A_{jj} \rangle = -\Gamma_j \langle \hat{A}_{jj} \rangle - i\Omega_j (\langle \hat{A}_{j0} \rangle - \langle \hat{A}_{0j} \rangle), \quad (16)$$

$$\begin{aligned} \frac{d}{dt} \langle A_{0j} \rangle = & -\left(i\delta_j + \frac{\Gamma_j}{2} \right) \langle \hat{A}_{0j} \rangle - i\Omega_j (\langle \hat{A}_{00} \rangle - \langle \hat{A}_{jj} \rangle) \\ & + i\Omega_k \langle \hat{A}_{kj} \rangle. \end{aligned} \quad (17)$$

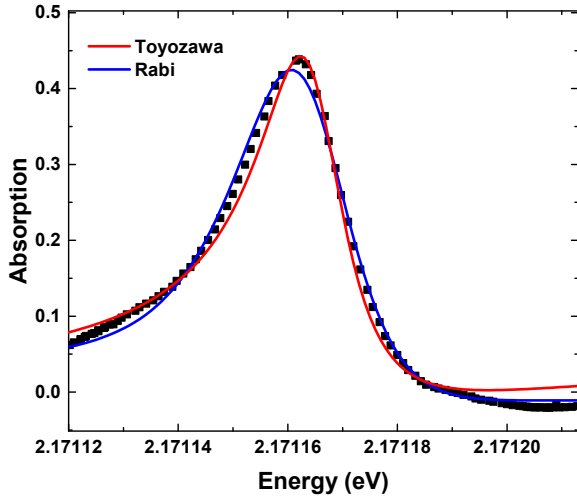


FIG. 6. Fitted absorption spectrum of the exciton resonance $n = 10$, with the Toyozawa and the Rabi-model.

Here, $k = (n + 1, n)$ for $j = (n, n + 1)$. Equation (16) and the first line of Eq. (17) represent the terms known from an isolated exciton resonance based on Eq. (5) from the main text. The only difference is due to the adjusted completeness relation

$$\hat{1} = \hat{A}_{00} + \hat{A}_{nn} + \hat{A}_{n+1, n+1}. \quad (18)$$

However, the second line in Eq. (17) stems from the laser driven resonance k and couples the two excited states. It is based on the common ground state of both resonances allowing an effective quadrupolar coupling via the intermediate state $|0\rangle$. The equation of motion for such a coupling $\langle \hat{A}_{kj} \rangle$ then reads as

$$\begin{aligned} \frac{d}{dt} \langle \hat{A}_{kj} \rangle &= - [i(\delta_j - \delta_k) + \frac{\Gamma_j + \Gamma_k}{2}] \langle \hat{A}_{kj} \rangle \\ &\quad - i\Omega_j \langle [\hat{A}_{kj}, \hat{A}_{j0}] \rangle - i\Omega_k \langle [\hat{A}_{kj}, \hat{A}_{0k}] \rangle \end{aligned} \quad (19)$$

$$\begin{aligned} &= - [i(\delta_j - \delta_k) + \frac{\Gamma_j + \Gamma_k}{2}] \langle \hat{A}_{kj} \rangle \\ &\quad - i\Omega_j \langle \hat{A}_{k0} \rangle + i\Omega_k \langle \hat{A}_{0j} \rangle. \end{aligned} \quad (20)$$

From the above, two effects couple the resonances n and $n + 1$, the completeness relation and the nonvanishing value of $\langle \hat{A}_{n, n+1} \rangle$.

Model for asymmetry parameter

As we do not yet have a full theory for the peak asymmetry q_n , we can use the following argument. According to Toyozawa [22], the asymmetry comprises couplings to all other excited states via a phonon background. For large n , one may assume that this coupling is rather insensitive as the main couplings to low- n states is almost the same for similarly large values of n . In this case the q_n in the Rabi model would become constant, $q_n \rightarrow q$ for $n \rightarrow \infty$. With this in mind, we can

set the Toyozawa and the Rabi spectrum equal and determine the apparent q_n fitted in the former. This yields

$$\begin{aligned} q_n &= g_n^2 \Omega_n^2 \frac{(\frac{\Gamma_n}{2})^2 + \delta_n^2}{[(\frac{\tilde{\Gamma}_n}{2})^2 + \delta_n^2]^2} q \\ &\quad + \frac{\Gamma_n}{4\delta_n} \left[1 - g_n^2 \Omega_n^2 \frac{(\frac{\Gamma_n}{2})^2 + \delta_n^2}{[(\frac{\tilde{\Gamma}_n}{2})^2 + \delta_n^2]^2} \right] \end{aligned} \quad (21)$$

Here, $\tilde{\Gamma}_n = \sqrt{(\sqrt{2} - 1)(\Gamma_n^2 + 8\Omega_n^2)}$ in order to include the different fitted widths from the two models. Unsurprisingly, q_n is now a function of ω_L , meaning that we can only evaluate it at certain laser frequencies. We thus evaluate the arithmetic average between the values at the two half width values $\delta_n = \pm \tilde{\Gamma}_n/2$. Including again the different n -dependencies, we obtain after some algebra

$$q_n = P \frac{1 + \alpha n^3}{(1 + 2\alpha n^3)^2} q, \quad (22)$$

with P and α positive constants. For $\alpha n^3 \ll 1$ we reobtain a constant behaviour of the apparent asymmetries, whereas for large n , even though q is constant q_n goes down to zero. This behaviour seems to be roughly confirmed by the experimental fitting to the Toyozawa spectrum, see Fig. 7.

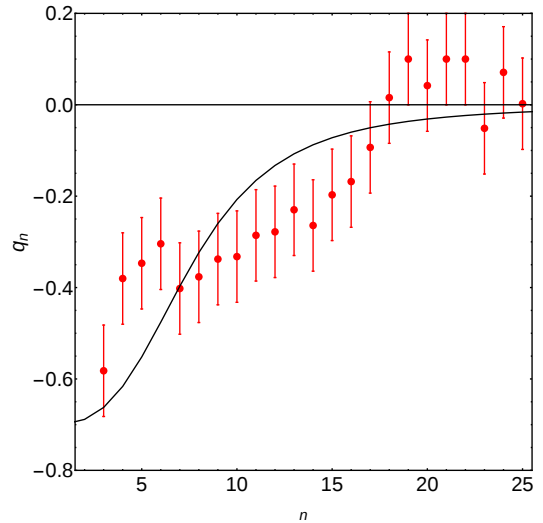


FIG. 7. Experimental fitting values for q_n from [5] (red dots), and theoretical curve according to Eq. (22) with $\alpha = 7 \times 10^{-4}$ and $P \cdot q = -0.7$ (black line). The q_n are depicted with an error estimate of ± 0.1 .

* Electronic address: peter.gruenwald@uni-rostock.de

- [1] D. Meschede, H. Walther, and G. Müller, *One-Atom Maser*, Phys. Rev. Lett. **54**, 551 (1985).
- [2] G. Rempe, H. Walther, and N. Klein, *Observation of quantum collapse and revival in a one-atom maser*, Phys. Rev. Lett. **58**, 353 (1987).

- [3] J. M. Raimond, M. Brune, and S. Haroche, *Manipulating quantum entanglement with atoms and photons in a cavity*, Rev. Mod. Phys. **73**, 565 (2001).
- [4] M. Saffman, T. G. Walker, and K. Mølmer, *Quantum information with Rydberg atoms*, Rev. Mod. Phys. **82**, 2313 (2010).
- [5] T. Kazimierczuk, D. Fröhlich, S. Scheel, H. Stolz, and M. Bayer, *Giant Rydberg excitons in the copper oxide Cu₂O*, Nature **514**, 343 (2014).
- [6] R. J. Elliott, *Symmetry of excitons in Cu₂O*, Phys. Rev. **124**, 340–345 (1961).
- [7] H. Haug and S.W. Koch, *Quantum Theory of the Optical and Electronic Properties of Semiconductors* (World Scientific, 2009).
- [8] J.R. Rydberg, *On the emission spectra of the chemical elements*, K. Svenska Vetensk. Akad. Handl. **23**, 11 (1889).
- [9] F. Schöne, S.-O. Krüger, P. Grünwald, J. Thewes, M. Aßmann, J. Heckötter, D. Fröhlich, M. Bayer, H. Stolz, and S. Scheel, *Deviations of the exciton level spectrum in Cu₂O from the hydrogen series*, Phys. Rev. B **93**, 075203 (2016).
- [10] F. Schöne, S.-O. Krüger, P. Grünwald, M. Aßmann, J. Heckötter, J. Thewes, H. Stolz, D. Fröhlich, M. Bayer, and S. Scheel, *Coupled valence band dispersions and the quantum defect of excitons in Cu₂O*, J. Phys. B: At. Mol. Opt. Phys. **49**, 134003 (2016).
- [11] A. Baldereschi and N. O. Lipari, *Spherical Model of Shallow Acceptor States in Semiconductors*, Phys. Rev. B **8**, 2697 (1973).
- [12] A. Baldereschi and N. O. Lipari, *Cubic contributions to the spherical model of shallow acceptor states*, Phys. Rev. B **9**, 1525 (1974).
- [13] J. Thewes, J. Heckötter, T. Kazimierczuk, M. Aßmann, D. Fröhlich, and M. Bayer, *Observation of High Angular Momentum Excitons in Cuprous Oxide*, Phys. Rev. Lett. **115**, 027402 (2015).
- [14] J. P. Reithmaier, G. Sek, A. Löffler, C. Hofmann, S. Kuhn, S. Reitzenstein, L. V. Keldysh, V. D. Kulakovskii, T. L. Reinecke, and A. Forchel, *Strong coupling in a single quantum dot-semiconductor microcavity system*, Nature **432**, 197 (2004).
- [15] T. Yoshie, A. Scherer, J. Hendrickson, G. Khitrova, H. M. Gibbs, G. Rupper, C. Ell, O. B. Shehkin, and D. G. Deppe, *Vacuum Rabi splitting with a single quantum dot in a photonic crystal nanocavity*, Nature **432**, 200 (2004).
- [16] A. Müller, E. B. Flagg, P. Bianucci, X. Y. Wang, D. G. Deppe, W. Ma, J. Zhang, G. J. Salamo, M. Xiao, and C. K. Shih, *Resonance Fluorescence from a Coherently Driven Semiconductor Quantum Dot in a Cavity*, Phys. Rev. Lett. **99**, 187402 (2007).
- [17] P. Grünwald, G. K. G. Burau, H. Stolz, and W. Vogel, *Superfluorescence spectra of excitons in quantum wells*, Phys. Rev. B **88**, 195308 (2013).
- [18] P. Grünwald and W. Vogel, *Enhanced Squeezing by Absorption*, Phys. Scr. **91**, 043001 (2016).
- [19] F. Richter, M. Florian, and K. Henneberger, *Generalized radiation law for excited media in a nonequilibrium steady state*, Phys. Rev. B **78**, 205114 (2008).
- [20] D. Yu. Vasylyev, W. Vogel, K. Henneberger, T. Schmielau and D.-G. Welsch, *Propagation of nonclassical optical radiation through a semiconductor slab*, Phys. Rev. A **78**, 033837 (2008).
- [21] S. Huppert, A. Vasanelli, T. Laurent, Y. Todorov, G. Pegolotti, G. Beaudoin, I. Sagnes, and C. Sirtori, *Radiatively Broadened Incandescent Sources*, ACS Photonics **2**, 1663 (2015).
- [22] Y. Toyozawa, *Interband effect of lattice vibrations in the exciton absorption spectra*, J. Phys. Chem. Solids **25**, 59 (1964).
- [23] C. Malerba, F. Biccari, C. L. A. Ricardo, M. D’Incau, P. Scardi, and A. Mittiga, *Absorption coefficient of bulk and thin film Cu₂O*, Sol. Energ. Mat. Sol. Cells **95**, 2848 (2011).
- [24] C. Matthiesen, A. N. Vamivakas, and M. Atatüre, “Subnatural Linewidth Single Photons from a Quantum Dot”, Phys. Rev. Lett. **108**, 093602 (2012).
- [25] W. Vogel and D.-G. Welsch, *Quantum Optics* (Berlin, Wiley-VCH, 2006).
- [26] B. R. Mollow, *Power Spectrum of Light Scattered by Two-level Systems*, Phys. Rev. **188**, 1969 (1969).
- [27] F. Schuda, C. R. Stroud Jr., and M. Hercher, “Observation of the resonant Stark effect at optical frequencies”, J. Phys. B **7**, L198 (1974).